

IMECE2016-66697

**ADDITIVELY MANUFACTURED COMPONENTS WITH EMBEDDED
INSTRUMENTATION**

Matthew Davis
Luna Innovations
Blacksburg, VA, USA

Dr. John Middendorf
Advratech
Dayton, OH, USA

Naman Garg
Luna Innovations
Blacksburg, VA, USA

Dr. Osgar John Ohanian III
Luna Innovations
Blacksburg, VA, USA

ABSTRACT

Additively manufactured components enable complex structures to be rapidly fabricated and tested for use in the automotive and aerospace industries. Additive manufacturing capabilities have expanded to include a variety of plastics, metal alloys, and fiber-reinforced polymers. There is interest in quantifying the residual stresses in components that have been manufactured using 3D printing processes in order to refine fabrication parameters and improve the performance of component design. Luna Innovations has developed and demonstrated methods to embed high definition fiber optic sensing (HD-FOS) technology into components that have been additively manufactured using ABS plastic as well as a cobalt chrome alloy. This technology enables characterization of internal residual stresses and provides a method for lifetime health monitoring of these printed components using the strain and temperature sensors installed during printing. The sensing technology utilizes the Rayleigh backscatter pattern contained in an optical fiber to determine the strain or temperature, with a high spatial resolution of 1.28 mm, along a fiber that can be embedded inside a printed component. HD-FOS technology was used to measure internal residual strains within layers of varying depths of an ABS printed block, showing a parabolic strain profile with a peak at 9,600 microstrain. In addition to characterizing the printing process, a method has been demonstrated to embed a distributed temperature sensor into a metallic additively manufactured component. This enables the temperature of the part to be measured while it is in use, providing data on the heat transfer through the component. Additive manufacturing has enabled embedding fiber optic

sensors in new configurations that were previously unobtainable.

INTRODUCTION

Additive Manufacturing (AM) is changing the way designers and fabricators think about creating parts. It is even changing the boundaries of what geometries can be manufactured. Researchers around the world are exploring the possibilities of what can be accomplished with AM that could not be attained with traditional manufacturing techniques. The motivation of this research is twofold: 1) to better understand physical phenomena taking place during 3D printing through embedding distributed sensors during the build process, and to 2) integrate fiber optics in structures to enable unprecedented sensing capabilities.

Additive manufacturing began with polymers as the base material, but has expanded to include metals [1] and even biological tissues and organs [2]. Additive manufacturing provides a novel solution to creating multifunctional designs, as other researchers have demonstrated embedding wires [3], integrated electronic circuits [4], antennas [5], sensors [7], digital displays [6], fiber optics [11], and even electric motor components [12].

The present research provides an innovative advancement based on the accomplishments of past research. Integration of high spatial resolution distributed temperature and strain sensing just below the surface of metal parts will enable robust sensing capabilities that were not previously attainable. This capability could benefit aerospace, automotive, medical, energy and industrial markets.

NOMENCLATURE

- AM: Additive Manufacturing
- CAD: Computer Aided Design
- OFDR: Optical Frequency Domain Reflectometry
- SLM: Selective Laser Melting

FIBER OPTIC SENSING TECHNIQUE

"The fiber optic sensors are manufactured from standard off-the-shelf telecommunications fiber with a Ge-doped fused silica core and fused silica cladding and a protective coating, typically a polymer (although metals are possible). An individual sensor can be tens of meters in length and provide thousands of measurements at configurable points distributed along its length. Measurements are made using the Rayleigh scatter in the fiber, a random but stable pattern of reflections inherent to each fiber as a result of small-scale non-homogeneities. This random pattern of reflections is unique to each fiber and constant for the life of the fiber, forming a reflection signature unique to each sensor. Strain or temperature results in an apparent stretching of this signature, which translates to a shift in the spectral content of the pattern. As both stimuli affect the fiber in a similar manner, sensors designed to measure temperature are mechanically isolated from strain by sheathing them in a PTFE, stainless steel, or other suitable tubing.

Sensors are interrogated using optical frequency domain reflectometry (OFDR), an interferometric technique that can distinguish scattering points at different locations along the fiber [8-10]. FIGURE 1 describes the basic OFDR network while FIGURE 2 walks through the steps taken to obtain, in this case, a strain measurement. Light from a swept-tunable laser is split between the measurement path and a reference path by a fiber optic coupler. Light in the measurement path is sent to the sensor through the input path of an optical coupler. Light reflected from the sensor returns through the coupler and is recombined with light from the reference path. This combined signal then passes through a polarization beam splitter, which splits the light into orthogonal states recorded at the S and P detectors. A Fourier transform of these signals yields the phase and amplitude of the signal as a function of length along the sensor, i.e., the sensor signature.

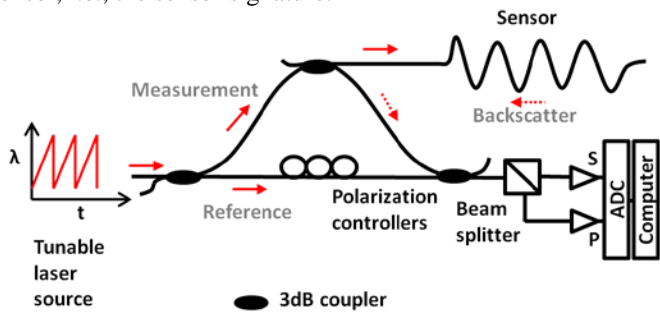


FIGURE 1. BASIC OFDR OPTICAL NETWORK[11][12].

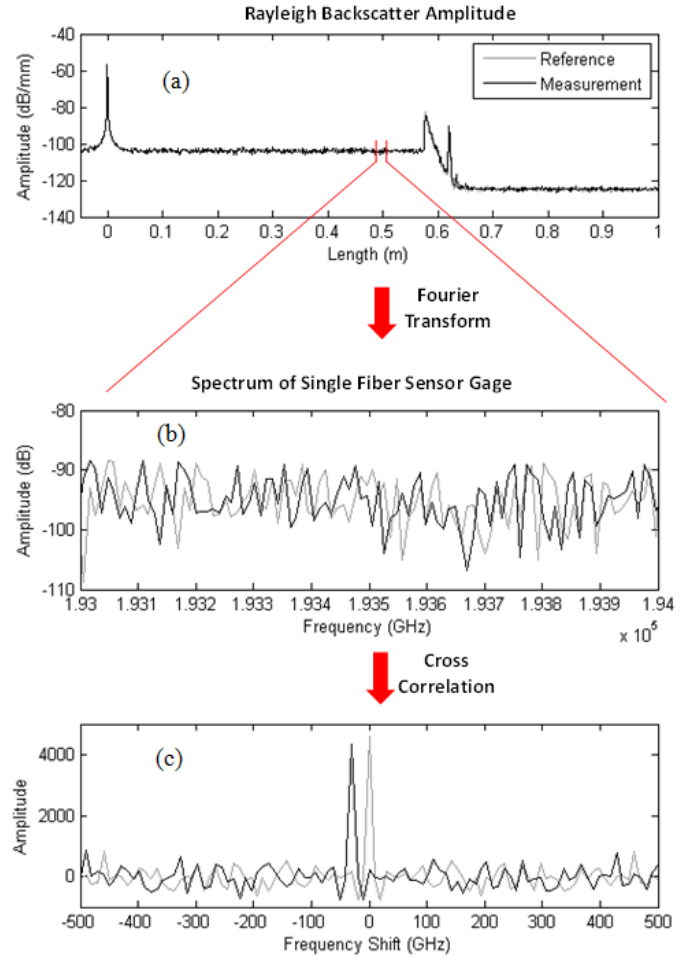


FIGURE 2. FREQUENCY SHIFT CALCULATION FROM RAYLEIGH SCATTER MEASUREMENT. (A) RAYLEIGH BACKSCATTER ALONG OPTICAL PATH. (B) SPECTRUM OF SINGLE SENSOR GAGE. (C) CROSS-CORRELATION OF REFERENCE AND MEASUREMENT SPECTRA. [12]

To calculate either a strain or temperature measurement, the spectral content of the sensor is compared between the measurement and reference state. Complex Fourier transform data is windowed around a desired measurement location (FIGURE 2(a)). This window determines the gage length of the measurement. An inverse Fourier transform of the windowed data gives the spectral content from a particular gage in the sensor (FIGURE 2(b)), which is cross-correlated (FIGURE 2(c)) with the spectrum from the same location of the sensor in a baseline state. Finally, the cross-correlated shift is converted to strain using an empirically determined calibration coefficient, or gage factor, analogous to that of the electrical strain gage. This process is repeated along the length of the sensor, forming a distributed measurement.[11][12]"

EMBEDDING FIBER INTO PRINTED ABS

The initial demonstration of embedding optical fiber into additively manufactured components focused on integration into ABS plastics. During the first trial a simple rectangular part measuring 1.5 x 4.0 x 0.13 inches (38 x 100 x 3.3 mm) was used to evaluate the placing of fiber into the ABS material. The part was printed using alternating 45° passes with a 100% fill. The printer was programmed to stop the head and raise it after a defined number of passes to allow installation of the fiber. Each pass was set to be approximately 0.016 in (0.40 mm) thick.

The fiber was installed during a pause after the first two layers were printed. To install the fiber it was placed near the centerline and secured to the printing table. Two additional layers were printed over the fiber before the next pause and a section of Teflon tubing was placed along the centerline. The Teflon contained a section of the same fiber for the purpose of temperature sensing. The diameter of the PTFE tube, .035 in (.90 mm), was too large for the print head to clear, resulting in a poor embedding into the sample. This can be seen in FIGURE 3, with the part on the printing table.

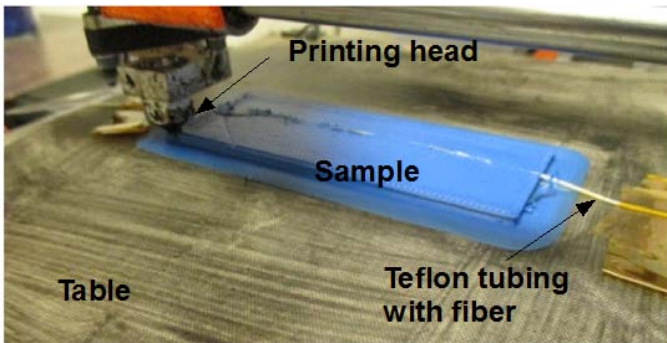


FIGURE 3: SAMPLE BEING PRINTED FROM ABS TO TEST FIBER EMBEDDING METHODS.

At this point the program was stopped and the part removed for evaluation. Data was not taken on this part during its fabrication. Its purpose was only to develop procedures. After fabrication, the sample part was sectioned for evaluation.

One side of the sectioned part was sanded to reveal the structure and interaction with the fiber and the PTFE. Care was taken to avoid overheating the part to prevent possible deformation due to elevated temperature during both the cutting and sanding stages. FIGURE 4 (left) shows the interaction with the PTFE tube, while FIGURE 4 (right) shows the fiber section which would be used for the strain sensing.

There did appear to be some minor voids between the passes of the ABS material. In a few cases those interstitial voids were relatively large. The ABS appeared to form well around the fiber and no interstitial voids were found at this one section, although they could exist at other locations. The Teflon was deformed during the process and was not circular. The printing head was at a temperature of approximately 500°F (260°C), which is also the maximum operating temperature for Teflon, suggesting the deformation could be due to short term

exposure to these temperatures. If this is the case and the Teflon was to deform and contract, it could impart a strain on the fiber. For other applications this could cause an error in the thermal compensation and should be further evaluated.

A large block sample was prepared in the same fashion as the previous sample. The basic schematic is shown in FIGURE 5, showing the planned fiber layout relative to the part's dimensions. The completed sample is shown in FIGURE 6. In this test, temperature sensors (i.e., Teflon sections) were avoided due to the limitation of small ABS bead size from the 3D printer. The challenges encountered with embedding Teflon sections in preliminary fabrication runs can be overcome by adjusting the model design to allow for small slots/gaps in the block sample. This allows Teflon segments to be embedded without impacting the printing process.

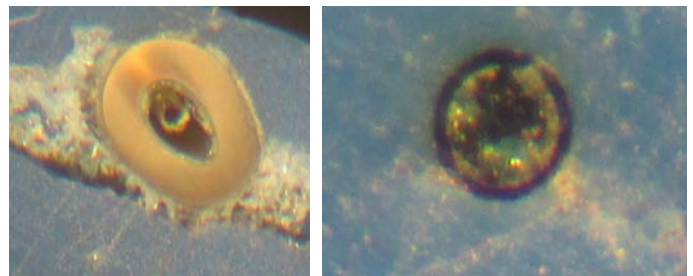


FIGURE 4: SECTION VIEW OF THE REGION WITH PTFE TUBING CONTAINING FIBER (LEFT). SECTION VIEW OF FIBER DIRECTLY EMBEDDED INTO THE MATERIAL.

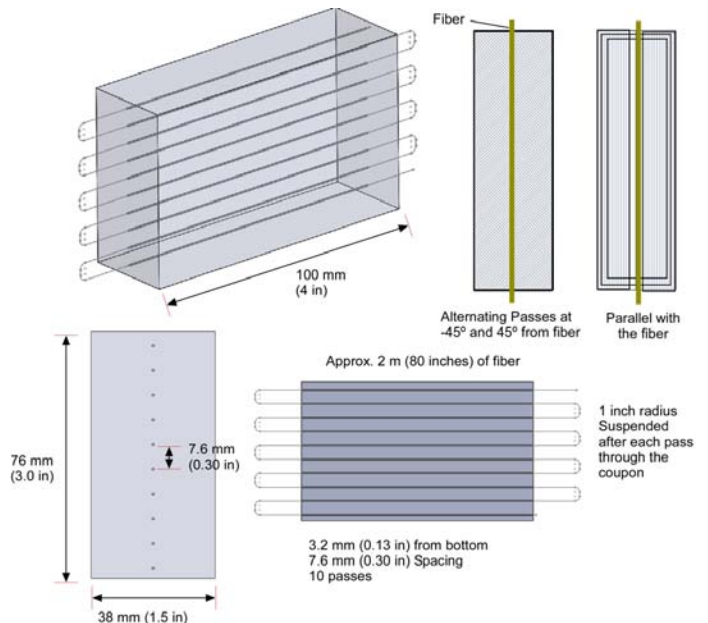


FIGURE 5: DESIGN OF THE LARGER ABS BLOCK USED FOR RESIDUAL STRAIN TESTING.

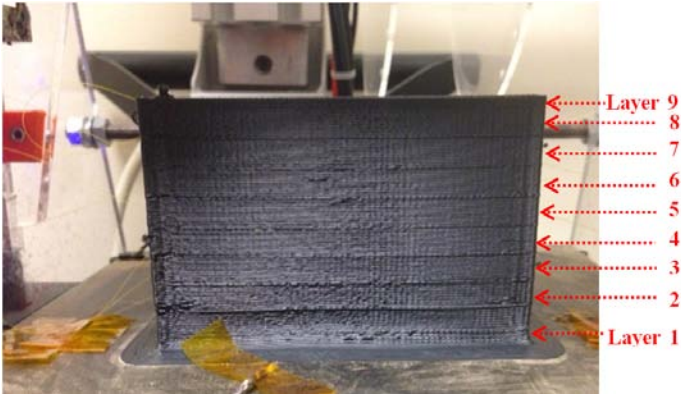


FIGURE 6: COMPLETED BLOCK WITH 9 LAYERS CONTAINING OPTICAL SENSING FIBER.

It is important to note that the final printed part is slightly different in size than what was shown in the schematic in Figure 5. Printing was stopped after a few layers were printed over the fiber segment in Layer 9, resulting in a total of nine embedded fiber segments. Dimensions of the final printed block were measured to be $\sim 3.8 \times 1.5 \times 2.5$ in. ($9.7 \times 3.8 \times 6.4$ cm). Approximately 19 layers were printed between each embedded fiber segment.

EMBEDDING INTO ADDITIVELY MANUFACTURED CO-CR ALLOY

There are many applications in which it is also desirable to embed sensors into metallic components. This would enable integrating sensors in locations that conventional machining techniques cannot access. Other applications include internal thermal mapping, which combined with a time resolved surface temperature measurement enables heat flux to be determined. There is also a need for long term structural health monitoring and the development of smart components.

The method employed to additively manufacture the metallic components was selective laser melting (SLM). This AM technology involves slicing a 3D CAD representation of a part into thin (.002 in [$50 \mu\text{m}$]) 2D layers, and then using a high power laser to melt an equally thin layer of powder into the 2D traces of that part. After a layer has been melted, a new layer of powder is spread over the first using a roller or scraper, and the next layer of the part is traced on top of the previous layer. As this process continues, the part is built upward; the 3D structure is made from many 2D slices. A graphical representation of this is given in FIGURE 7.

The SLM process is well established in the AM field and offers several advantages compared to other AM technologies. First, the laser used to melt the powder is focused onto a small spot and melts the metal very quickly. This localizes the area of heating, allowing for very small melt pools to be formed, which in turn increases the accuracy with which part geometries can be fabricated. Second, when the laser melts the metal powder, it forms one solid melt pool, which creates a very dense part with good mechanical properties. Another advantage with SLM is

that the process is easily scalable: a large part can be made as easily as a small part. The only limitation is the size of the build platter in the SLM machine. Of course, AM processes (including SLM) all have the advantage over traditional machining that a production line and special tooling are not needed. The only necessary components are metal powder and a CAD file.

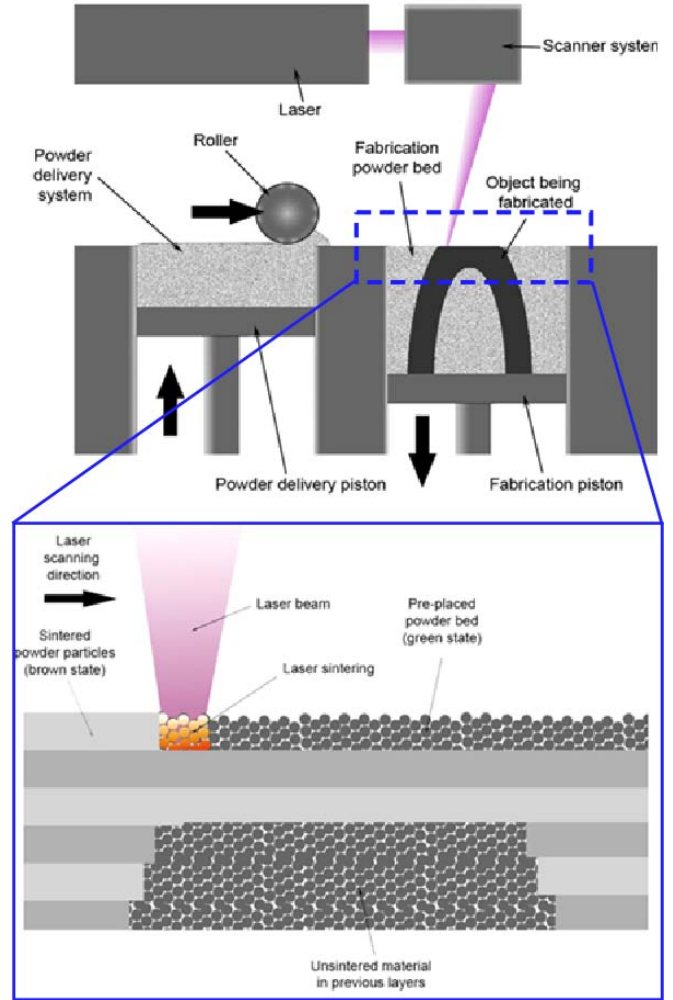


FIGURE 7: SCHEMATIC OF THE SLM PROCESS

The first step in the development of a method to integrate the sensing fiber for a strain measurement was to determine the amount of thermal input necessary to adhere the fiber to the alloy without damaging its ability to transmit light. For this testing, fiber coated with gold was selected. The gold coating will form a bond to the Co-Cr alloy as it is melted, enabling strain transfer to the fiber when the completed component is placed under a structural load.

The laser raster speed and power were varied as beads were melted over different sections of optical fiber to identify the range of suitable embedding parameters. This allowed researchers to analyze how the (gold) fiber coating reacted to several different heat input levels. FIGURE 8(a) shows the

single beads on the fiber and FIGURE 8(b) shows the wider passes varying the raster scan. From left to right, the raster (or scan) speed of the laser varies from 67 to 20 in/s (1700 to 500 mm/s), in 7.9 in/s (200 mm/s) increments. For these 7 speeds, the laser power is also varied from 80 to 40% in 10% increments, creating a total of 35 single beads over the fiber. None of the single beads presented obvious damage to the fiber; however, due to the short length it was not possible to evaluate them for optical continuity. The result is promising because it demonstrated that these fibers could be welded into AM components without being destroyed by the laser or the CoCr melt pool.

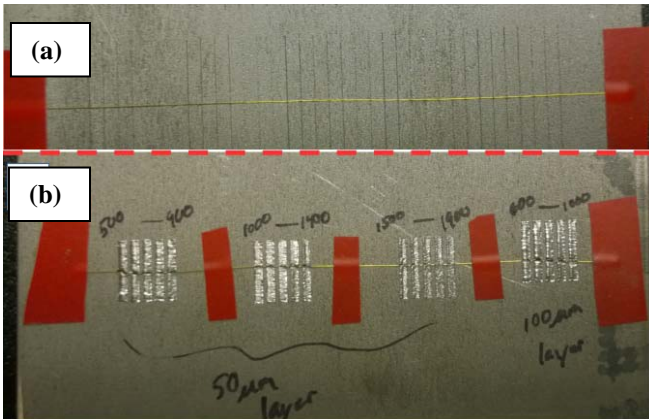


FIGURE 8: TESTS CONDUCTED TO DETERMINE THE APPROPRIATE POWER LEVELS FOR THE SLM SYSTEM.

The next step was to determine a method of integrating the fiber in which mechanical strain would not be coupled to the fiber for temperature sensing. A simple channel was printed into a layer of the component, and the fiber was installed into the channel. After installation, the remaining layers of the part were printed, covering the fiber.

The design of the channel began by investigating how the fiber channel width, as built by the SLM system, compares to the channel width in the original CAD file. The theoretical and experimental channel widths are different since the melt pool has a diameter associated with it. As the laser traces the exact width specified in the CAD file, the actual melted width will be the CAD specified width plus the melt pool diameter. The melt pool diameter is difficult to track accurately, so this issue was most easily resolved experimentally.

To find channel widths that would fit the fiber optic sensor a test specimen with 4 channels of varying width (FIGURE 10(a)) was created. The theoretical channel widths were 0.02, 0.03, 0.04, and 0.06 in. (500, 750, 1000, and 1500 μm). After the channels were constructed using the SLM the widths were quite smaller. A section of stainless steel tubing ~ 0.021 in. (530 μm) in diameter, used for sizing purposes, fit snugly into the 0.039 in (1000 μm) channel as shown in FIGURE 10(a). Similarly, the 0.006 in. (160 μm) diameter fiber was able to fit easily, but not loosely, into the 0.04 in. (750 μm) channel. This result indicates that the melt pool was ~ 0.019 in. (470 μm).

However, the fully melted portions of the part often have partially melted, or sintered, particles attached to them that also narrow the channel. These sections can be removed through a variety of methods to ensure that a uniform material forms the channel.

The next experiment for optimizing channel parameters was to determine how deep a melt pool over the channel would propagate towards the fiber in the channel. This simulates what will happen when the Co-Cr melts over the fiber channel, thereby embedding the fiber. By determining the melt depth over the channel, the bottom of the melt pool can be aligned with the top of the fiber while experiencing minimal thermal input. The melt depth test specimen is shown in FIGURE 9(b), and the resulting confocal microscope measurement can be seen in FIGURE 9(c). Measurements show that the molten CoCr penetrated ~ 0.023 in. (585 μm) into the 0.039 in. (1000 μm) deep channel. A similar melt depth was observed for the smaller fiber channels.

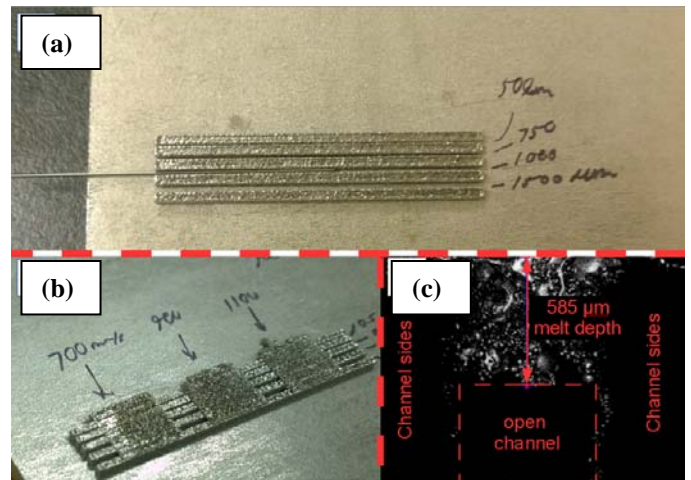


FIGURE 9: ITERATIONS PERFORMED TO DETERMINE THE CHANNEL PARAMETERS.

With the geometrical parameters identified for the channels that contain the fiber, several representative geometries were designed. These included an "L" shaped bracket, a hemisphere, and a wedge. Each of these designs were constructed and can be seen in FIGURE 10. Several of these components were separated from their build plates and used for thermal testing. Another component (not shown) was fabricated out of Ti-64 alloy to demonstrate that the same construction methods were applicable to additional alloys.

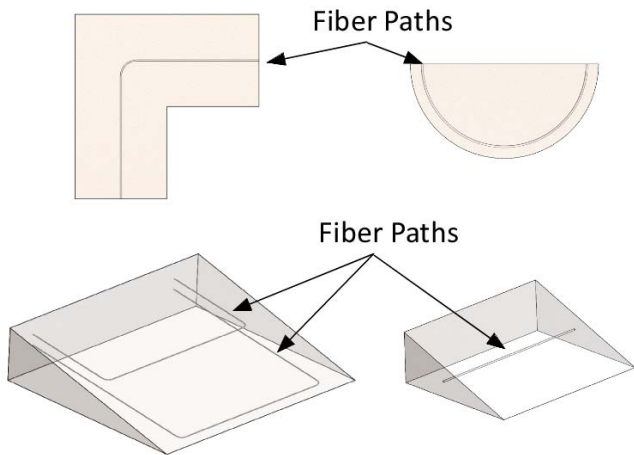


FIGURE 10: CONCEPTUAL IMAGES SHOWING THE APPROXIMATE LOCATIONS OF THE FIBER WITHIN THE SAMPLES (TOP). COMPLETED SAMPLES OF DIFFERENT GEOMETRIES WITH EMBEDDED FIBER OPTIC SENSORS (BOTTOM).

EXPERIMENTAL RESULTS - ABS

The block printed in ABS was evaluated to determine the amount of residual strain contained in the structure once it had returned to room temperature. Data taken on the sensor in an unstrained condition prior to being embedded was compared to the data taken after the part has cooled. The plot in FIGURE 11 shows the average strain from each embedded fiber segment plotted along the height (inches) of the printed block. A parabolic fit was performed to highlight the interesting strain profile as a function of height along the block from top to bottom. The results clearly show that the highest residual strains are towards the center of the block whereas the edges see up to 50% less strain in some cases. This could be a function of the combination of the fixed boundary condition at the point of attachment to the platen, free condition at the top, and the

cooling rates of the block during the printing. More testing would need to be performed to complete the evaluation for this specific geometry.

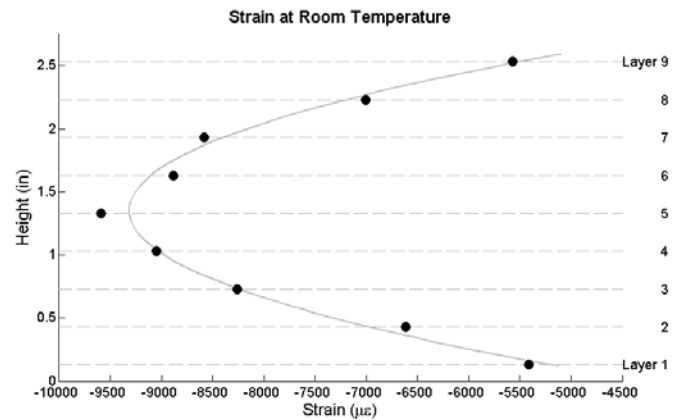


FIGURE 11: THE RESIDUAL STRAIN PROFILE OF THE LARGE 3D PRINTED ABS BLOCK.

EXPERIMENTAL RESULTS - METALLIC ALLOY

Three experiments were conducted with the Co-Cr additively manufactured metal components. These tests included a stepped thermal cycle, a high temperature soak, and a transient torch test.

Stepped Thermal Cycle

In the first test, one of the wedges was placed into a small furnace and heated in steps of 212 °F to 572 °F (100 °C to 300 °C). K-Type thermocouples were placed on the test article as a means of comparison for the measurement from the optical fiber (FIGURE 12). Data was collected with a spatial resolution of 0.05 in (1.28 mm) along the fiber sensor compared to the single point of the thermocouple.

Measurement Region of Interest

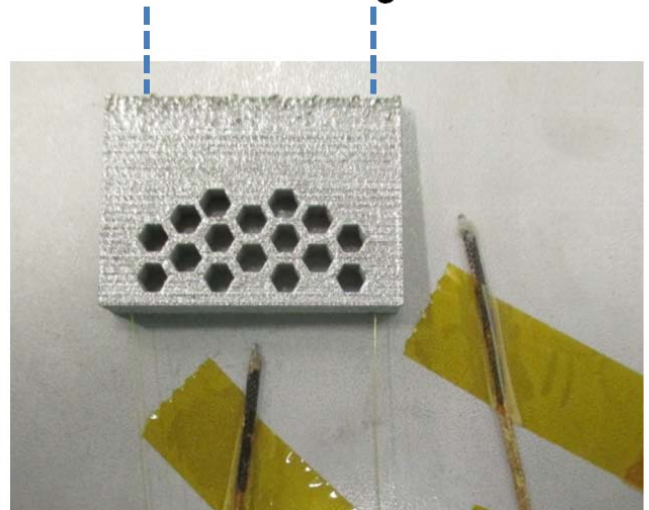


FIGURE 12: TEST ARTICLE SHOWING THE MEASUREMENT REGION OF INTEREST.

FIGURE 13 contains all of the data taken during the test, including the transient data between temperature points. A linear fit was applied to the data acquired during the steady state portions of the experiment indicated as calibration points within the figure. The linearity of the data, a slope of 1.012, can be used to demonstrate the accuracy of the measurement. Apparent error during the transient periods is due to the differing transient responses of the fiber located inside the component and the thermocouple directly exposed inside of the furnace hot zone.

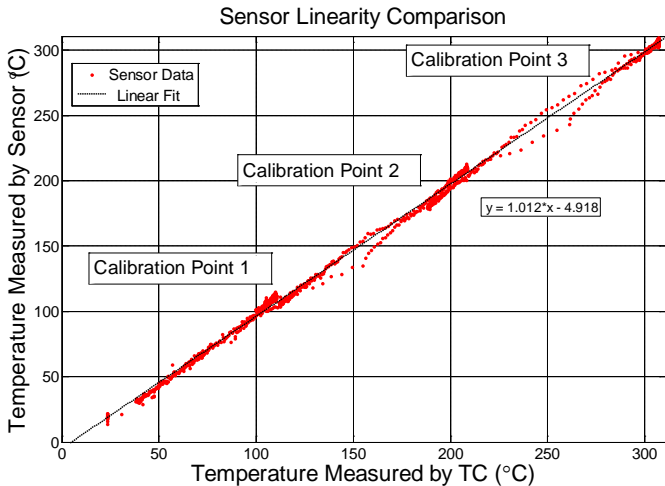


FIGURE 13: DATA FROM THE 300°C TEMPERATURE CYCLE USED FOR ACCURACY DETERMINATION.

High Temperature Soak

The second test evaluated the thermal stability of the sensing method inside of a small wedge while held at a constant temperature of 1022 °F (550 °C) over a period of 5 hours. During this time the fiber optic measurements from 10 points contained within the test article recorded an average temperature of 1018 °F (548.2 °C) while the thermocouple recorded an average of 1023 °F (551.0 °C). This places both measurements within 0.5% of each other over the measured range. The standard deviation of all 10 fiber measurements was 6.1 °F (3.4 °C) compared with a standard deviation of 2.9 °F (1.6 °C) on the thermocouple. The experimental results are plotted in FIGURE 14.

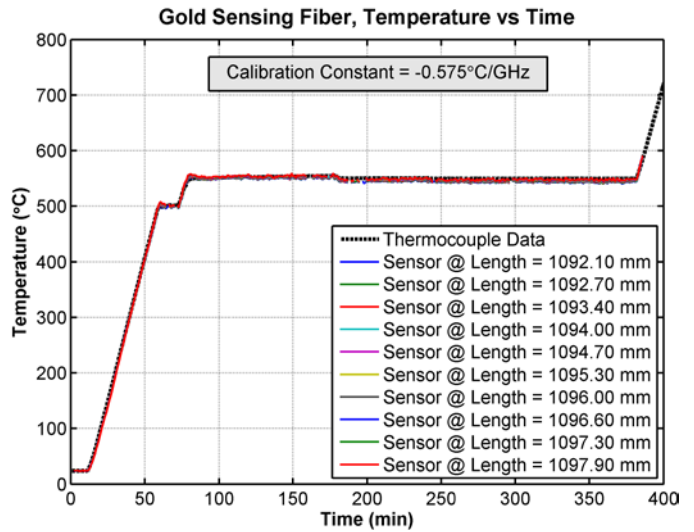


FIGURE 14: DATA FROM THERMAL STABILITY TESTING AT 550 °C OVER A 5 HOUR TIMEFRAME.

Transient Torch Experiment

The final test demonstrated the transient response of a component. This was accomplished by fixturing the test article in a small vice and heating it with an oxy-propane torch. Data was collected at a rate of 23 Hz with a spatial resolution of 0.05 in (1.28 mm) along the embedded fiber. The test article being heated can be seen in FIGURE 15.

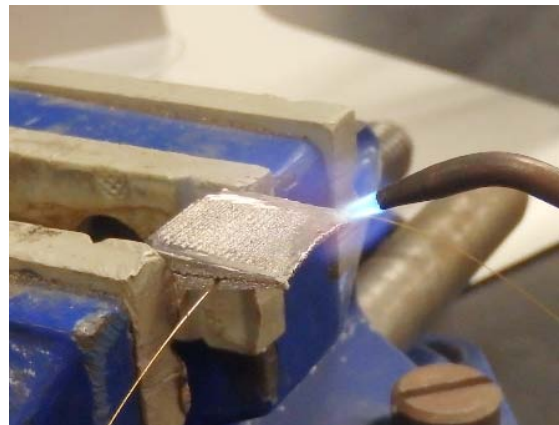


FIGURE 15: SAMPLE FIXTURED IN A SMALL VICE AND BEING HEATED WITH AN OXY-PROPANE TORCH.

FIGURE 16 displays selected time intervals over the first second of heating. In the figure the x-axis represents the measurement location on the fiber sensor as a function of length. Position 1.09 m is approximately at the center of the test article. Temperature is displayed on the y-axis as measured at each point for the time intervals selected.

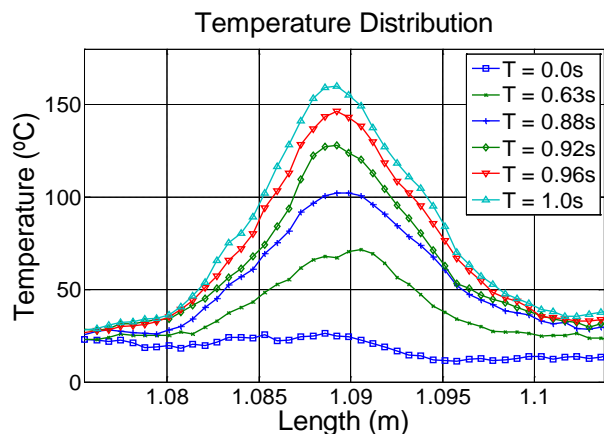


FIGURE 16: DATA AT SEVERAL TIME STEPS OF THE TEST ARTICLE BEING HEATED.

CONCLUSION

Through a series of experiments Luna and Advrtech researchers have demonstrated that optical fiber can be embedded into both 3D printed plastic materials and additively manufactured alloys, so that distributed strain and temperature measurements may be made along selected paths through the part. Experimental data was used to verify that the sensing method was accurate in the presence of temperature when compared to co-located thermocouples. Future development includes refining the embedding methods and applying them to specific components, and identifying techniques to mechanically protect fiber ingress/egress points. Testing will also be performed to evaluate the strain response of the technique. HD-FOS technology has the ability to enable the fabrication of smart components with embedded instrumentation which do not rely on conventional machining techniques. The high spatial resolution data can provide insight into structural loading and heat transfer on components integrated with the fiber optic sensing technology.

ACKNOWLEDGMENTS

Portions of the work presented in this paper were based upon work supported by the United States Air Force, FA9550-15-C-0034. Any opinions, findings and conclusions or recommendations expressed in this material are those of the author(s) and do not necessarily reflect the views of the United States Air Force

REFERENCES

- [1] Frazier, William E. "Metal additive manufacturing: a review." *Journal of Materials Engineering and Performance* 23, no. 6 (2014): 1917-1928.
- [2] Melchels, Ferry PW, Marco AN Domingos, Travis J. Klein, Jos Malda, Paulo J. Bartolo, and Dietmar W. Hutmacher. "Additive manufacturing of tissues and organs." *Progress in Polymer Science* 37, no. 8 (2012): 1079-1104.
- [3] D. Espalin, D. Muse, F. Medina, E. MacDonald and R. Wicker, "3D Printing Multi-Functionality: Structures with Electronics,"

- International Journal of Advanced Manufacturing Technology, vol. 72, no. 5-8, pp. 963-978, 2014.
- [4] C. Gutierrez, R. Salas, G. Hernandez, D. Muse, R. Olivas, E. MacDonald, M. Irwin, R. Wicker, M. Newton, K. Church and B. Zufelt, "CubeSat fabrication through additive manufacturing and micro-dispensing," *International Symposium on Microelectronics.*, vol. 2011, no. 1, 2011.
- [5] J. J. Casanova, J. A. Taylor and J. Lin, "Design of a 3-D fractal heatsink antenna," *IEEE Antennas and Wireless Propagation Letters*, vol. 9, pp. 1061-1064, 2010.
- [6] K. Willis, E. Brockmeyer, S. Hudson and I. Poupyrev, "Printed optics: 3D printing of embedded optical elements for interactive devices," in *25th annual ACM symposium on User interface software and technology*, 2012.
- [7] Siggard, Erik J., Anand S. Madhusoodanan, Brent Stucker, and Brandon Eames. "Structurally embedded electrical systems using ultrasonic consolidation (UC)." In *Proceedings of the 17th solid freeform fabrication symposium*, pp. 14-16. 2006.
- [8] Soller, B., Gifford, D., Wolfe, M., and Froggatt, M. "High resolution optical frequency domain reflectometry for characterization of components and assemblies." *Optics Express* 13 (2005): 666-674.
- [9] Soller, B. J., Wolfe, M., and Froggatt, M. E. "Polarization resolved measurement of Rayleigh backscatter in fiber-optic components." *Optical Fiber Communication Conference and Exposition and the National Fiber Optic Engineers Conference Technical Digest*. Anaheim, California, March 6, 2005. Optical Society of America, 2005. Paper NWD3. CD-ROM.
- [10] Kreger, S., Gifford, D. K., Froggatt, M. E., Soller, B. J., and Wolfe, M. S. "High resolution distributed strain or temperature measurements in single- and multi-mode fiber using swept-wavelength interferometry." *Optical Fiber Sensors, OSA Technical Digest*. Cancun, Mexico, October 23, 2006. Optical Society of America, 2006. Paper ThE42. CD-ROM.
- [11] Matt Castellucci, Sandra Klute, Evan M. Lally, Mark E. Froggatt, and David Lowry. "Three-axis distributed fiber optic strain measurement in 3D woven composite structures", *Proc. SPIE 8690, Industrial and Commercial Applications of Smart Structures Technologies 2013*, 869006 (March 29, 2013)
- [12] Nur Aida Abdul Rahim, Matthew A. Davis, Luke Routhier, Jason Chevalier, Joseph Bos, Stephen Kreger, and Eric Sanborn. "Accuracy and Survivability of Distributed Fiber Optic Temperature Sensors", *53rd AIAA Aerospace Sciences Meeting, AIAA SciTech*
- [13] R. R. Maier, W. N. MacPherson, J. S. Barton, M. Carne, M. Swan, J. N. Sharma, S. K. Futter, D. A. Knox, B. J. Jones and S. McCulloch, "Embedded fiber optic sensors within additive layer manufactured components.," *IEEE Sensors Journal*, vol. 13, no. 3, pp. 969-979, 2013.
- [14] E. Aguilera, J. Ramos, D. Espalin, F. Cedillos, D. Muse, R. Wicker and E. MacDonald, "3D printing of electro mechanical systems," in *Solid Freeform Fabrication Symposium*, 2013.